Metals and Materials International (2021) 27:2656–2665
https://doi.org/10.1007/s12540-020-00617-9

# Effect of Mn Content on the Characteristics of Inclusions in Ti-Containing Steel Welds

**Bingxin Wang**[1] · **Jing Li**[1]

Received: 14 November 2019 / Accepted: 8 January 2020 / Published online: 29 January 2020


**Abstract**
Steel weld metals containing Ti were prepared with Mn contents of 0.35%–2.98%. The inclusion characteristics in the weld metals were investigated by means of thermodynamic calculations coupled with electron probe microanalyses and transmission electron microscopy. The results show that with an increase in Mn content, the primary constituent phases of the inclusions are changed from pseudobrookite to a combination of pseudobrookite and spinel and eventually to a mixture of (Mn–Si–Al)-oxide, spinel and ilmenite. $Ti_3O_5$, $MnTi_2O_4$ and $MnTiO_3$ are the primary constituents of the pseudobrookite, spinel and ilmenite solid solutions, respectively. Spinel and ilmenite have higher amounts of Mn but lower amounts of Ti compared with that of pseudobrookite. The formation of large amounts of ilmenite and spinel leads to the development of a Mn-depleted zone (MDZ) in the vicinity of the matrix/inclusion interface. Acicular ferrite has a Baker–Nutting orientation relationship with $MnTi_2O_4$.

**Keywords** Weld metal · Oxide inclusion · Manganese content · Manganese depletion · Baker–Nutting orientation relationship

## 1 Introduction

It is common knowledge that acicular ferrite (AF) formation is strongly promoted by Ti-containing oxide inclusions in weld metals and/or steels [1–5]. The literature indicates that TiO can induce the nucleation of AF because of the appearance of a Baker–Nutting orientation relationship between TiO and AF [6, 7]. Several researchers [8–12] have reported that a Mn-depleted zone near $Ti_2O_3$ inclusions can be observed; thus, the inclusions promote AF nucleation by increasing the chemical driving force due to the depletion of Mn. The above results were indicated by Shim et al. in a steel-$Ti_2O_3$ diffusion bonding experiment [13].

However, in the case of the chemical compositions of commercial steels and/or ordinary weld metals, complex Ti-containing oxide inclusions, such as $MnTi_2O_4$ and $MnTiO_3$, rather than the simple inclusions mentioned above, are usually formed [14–17]. Therefore, it is much more meaningful to investigate the potency of complex Ti-containing oxide inclusions to nucleate intragranular AF. Some researchers have performed related investigations. Kang et al. [16] and Nako et al. [18] pointed out that inclusions with a $MnTi_2O_4$ phase had a strong ability to promote AF nucleation by crystallographic lattice matching. Kang et al. [14–16] showed that the formation of large amounts of $MnTi_2O_4$ and $MnTiO_3$ phases in inclusions can consume Mn in the matrix near inclusions, which results in the formation of AF by a Mn-depletion mechanism.

Therefore, the formation of Ti-containing inclusions mentioned above is essential for AF nucleation regardless of Mn depletion or crystallographic lattice matching mechanisms; additionally, being able to accurately control the formation of such inclusions is very important. The chemical compositions of steels and/or weld metals have a strong effect on the formation, types and structures of inclusions. Kang et al. [14] studied the evolution of Ti-containing inclusions and pointed out that a Ti-rich oxide changed from a $MnTi_2O_4$-rich spinel to a mixture of $Ti_2O_3$ and $MnTiO_3$, and the $Ti_2O_3$ content increased with increasing Ti content. Moreover, some researchers have also investigated the influences of Al [19], Zr [19, 20], Mg [21], etc., on inclusion formation. Mn is one of the most basic constituents in the chemical compositions of steels and/or weld metals for

✉ Bingxin Wang
wangbingxin@163.com

[1] College of Mechanical Engineering, Liaoning Shihua University, Fushun 113001, China

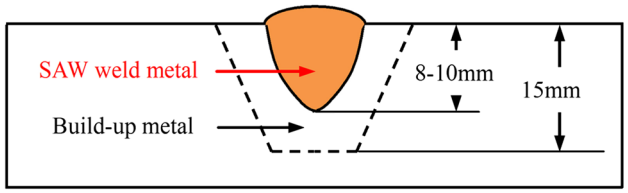


**Fig. 1** Schematic drawing showing the preparation of the weld metal

**Table 1** Chemical compositions of the welding wire (mass%)

| C | Mn | Si | S | P | Al |
|---|---|---|---|---|---|
| 0.05 | 0.86 | 0.06 | 0.022 | 0.02 | 0.01 |

structural applications. However, few studies have investigated the effect of Mn on the characteristics of inclusions in Ti-containing weld metals.

The present study analyzed how Mn affects the characteristics of inclusions, including the types, contents and chemical compositions for the constituent phases of inclusions in Ti-containing steel weld metals, using a FactSage commercial thermochemical computing package combined with an electron probe microanalyzer and transmission electron microscopy.

## 2 Experimental procedures

Figure 1 indicates the process of weld metal preparation. Build-up welding using pure Fe powder was first performed in a 15 mm deep trapezoidal slot in C-Mn steel plates with a thickness of 20 mm, and then a V-groove with a depth of 7 mm was machined at the build-up welds. After that, H08MnA welding wire (4 mm in diameter) was used in a submerged-arc welding process that was applied under the following conditions: a single pass, a voltage of 30 V, and an electric current of 460 A. The weld metals containing three kinds of Mn contents but with almost the same Ti concentrations were prepared by filling different amounts of Mn–Fe powder (81% Mn) and a certain amount of Ti-Fe powder (33% Ti) into the groove before welding. In the meantime, small amounts of pure Cr powder and Mo-Fe powder (55.18% Mo) were also added to keep the hardenability of the weld metals constant. Using an optical emission spectrometer (OES-5500, Shimadzu), the compositions of the above weld metals were analyzed, and nitrogen and oxygen were analyzed using a Leco TC-436 N/O analyzer. The compositions of the welding wire and weld metals are shown in Tables 1 and 2, respectively. According to the levels of Mn, weld metals were marked as WL (0.35% Mn), WM (1.05% Mn) and WH (2.98% Mn).

The specimens were machined along the welding direction, and the planes for examination were perpendicular to the welding direction. An electron probe microanalyzer (EPMA, JEOL JXA-8530F) was used to analyze the morphology and chemical elements of the inclusions after mechanical polishing of the specimens. Three inclusions in each weld metal were investigated. After the above specimens were etched with 4% Nital solution, the weld microstructures were examined by a Leica DMIRM image analyzer.

Transmission electron microscopy (TEM) analysis was conducted to identify phases in the inclusions using selected area electron diffraction (SAED) patterns and energy dispersive spectroscopy (EDS). Slices with a thickness of 0.3 mm were first mechanically thinned to 80 μm, and then twin-jet electropolishing was carried out using an electrolyte containing 8% perchloric acid and 92% ethanol at − 30 °C. After that, thin foil specimens were finally obtained after some ion milling steps and were analyzed by an FEI Tecnai G2 F20 TEM with an operating voltage of 200 kV.

The Mn concentration profile was measured by an EDS spot analysis at intervals of 10 nm from the inclusion/matrix interface, as shown in Fig. 2. Five measurements were conducted for every 10-nm interval, and average values for Mn content along with the confidence intervals under a confidence level of 95% were calculated.

The formation of inclusions in weld metals with different Mn contents was analyzed by a FactSage™ (version 7.2) thermochemical computing package using the FToxid, FTmisc and FSstel databases. According to the chemical compositions of the weld metals and selected databases, the following major constituent phases of the inclusions are considered for the thermochemical calculations:

Pseudobrookite: $Ti_3O_5$–$FeTi_2O_5$–$MnTi_2O_5$ solid solution
Spinel: $(Mn, Fe)(Ti, Al)_2O_4$ solid solution
Ilmenite: $Ti_2O_3$–$FeTiO_3$–$MnTiO_3$ solid solution
Mullite: $Al_2Si_1O_5$–$Al_2Al_1O_5$ solid solution
Corundum: $Al_2O_3$ + ($Ti_2O_3$ in dilute amount)

**Table 2** Chemical compositions of the weld metals (mass%)

| C | Mn | Si | Cr | Mo | S | P | Al | O | N | Ti |
|---|---|---|---|---|---|---|---|---|---|---|
| 0.035 | 0.35 | 0.14 | 1.58 | 1.27 | 0.028 | 0.032 | 0.011 | 0.040 | 0.0037 | 0.029 |
| 0.044 | 1.05 | 0.15 | 0.65 | 1.31 | 0.027 | 0.035 | 0.012 | 0.039 | 0.0041 | 0.030 |
| 0.060 | 2.98 | 0.15 | 0.11 | 0.15 | 0.024 | 0.039 | 0.012 | 0.037 | 0.0039 | 0.025 |

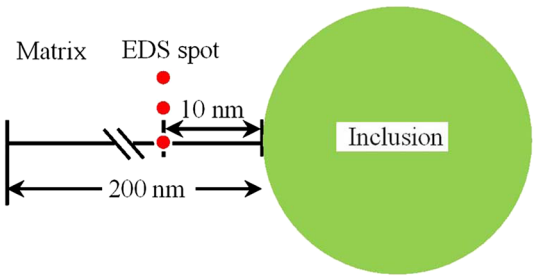


**Fig. 2** Schematic drawing indicating the measurement of Mn concentration by EDS within a range of 200 nm from the inclusion/matrix interface

Stoichiometric compounds: all relevant stoichiometric compounds, namely, $Mn_2Al_4Si_5O_{18}$, $Mn_3Al_2Si_3O_{12}$ and MnS

Slag phase: $Al_2O_3$–$Ti_2O_3$–$TiO_2$–MnO–$SiO_2$–FeO multiconstituent liquid oxide solutions resulting from the oxidation reactions of Si, Al, Mn, Ti, etc., in weld metals

An equilibrium cooling mode was used to calculate the formation of inclusions between 1000–1600 °C. Moreover, for the sake of simplicity, the thermodynamic calculation did not involve various solid-state transitions and reactions during further cooling.

The MnO–$TiO_x$ oxide system is very important due to the formation of a variety of Ti-containing oxide inclusions that are effective for intragranular AF nucleation. A phase diagram module was used to generate a ternary isothermal phase diagram at 1000 °C for the system containing MnO–$TiO_x$ components to study the effect of Mn on the formation of complex MnO–$TiO_x$ inclusions.

## 3 Results and Discussion

Microstructural variations with different Mn contents in the weld metals are shown in Fig. 3. It is clearly evident that when the Mn content in the weld metal increases, the AF amount increases and the amounts of the side plate and bainitic ferrites decrease.

Figure 4 shows the EPMA maps of the chemical element distribution for the typical inclusions in the weld metals with different levels of Mn. On the basis of the chemical composition characteristics shown in the EPMA analysis results of the inclusions, the inclusions in the three kinds of weld metals all contain (Mn–Si–Al)-oxide, (Mn–Ti)-oxide, Al-containing oxide and MnS constituents. However, the amounts of some constituents are changed in weld metals with different Mn contents. The inclusion in WL contains a large amount of (Mn–Ti)-oxide in addition to a small amount of (Mn–Si–Al)-oxide. In WM, the constituent phases of the

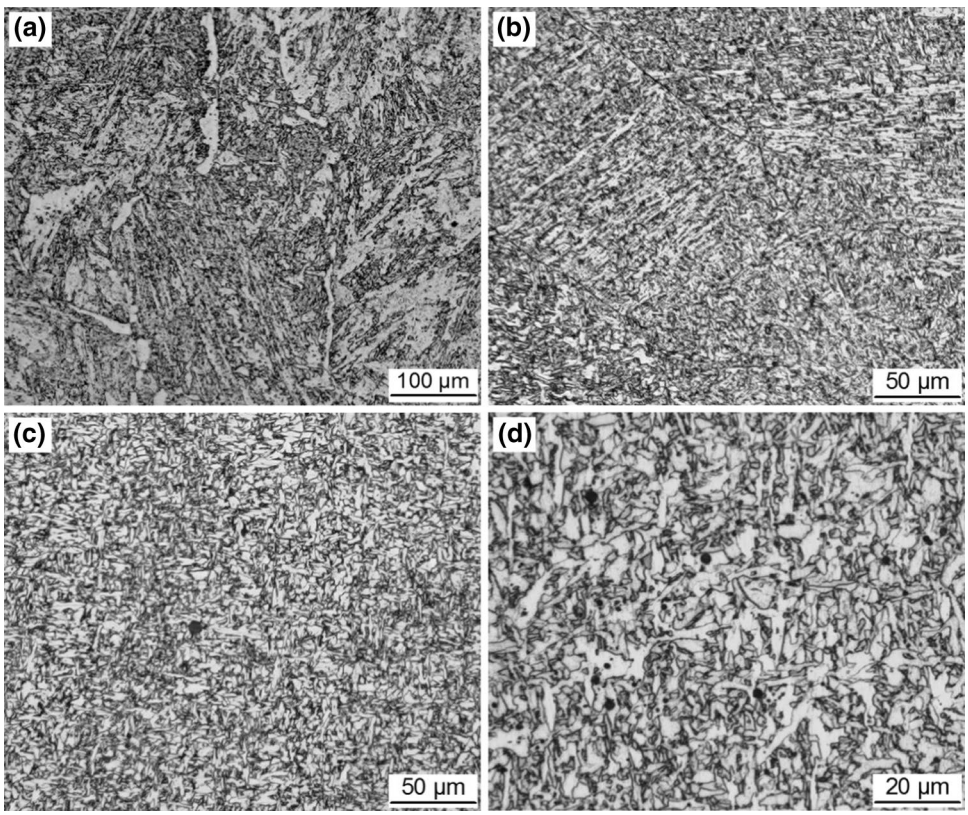


**Fig. 3** Metallographic microstructures of **a** WL, **b** WM, **c** WH, and **d** WH under amplification

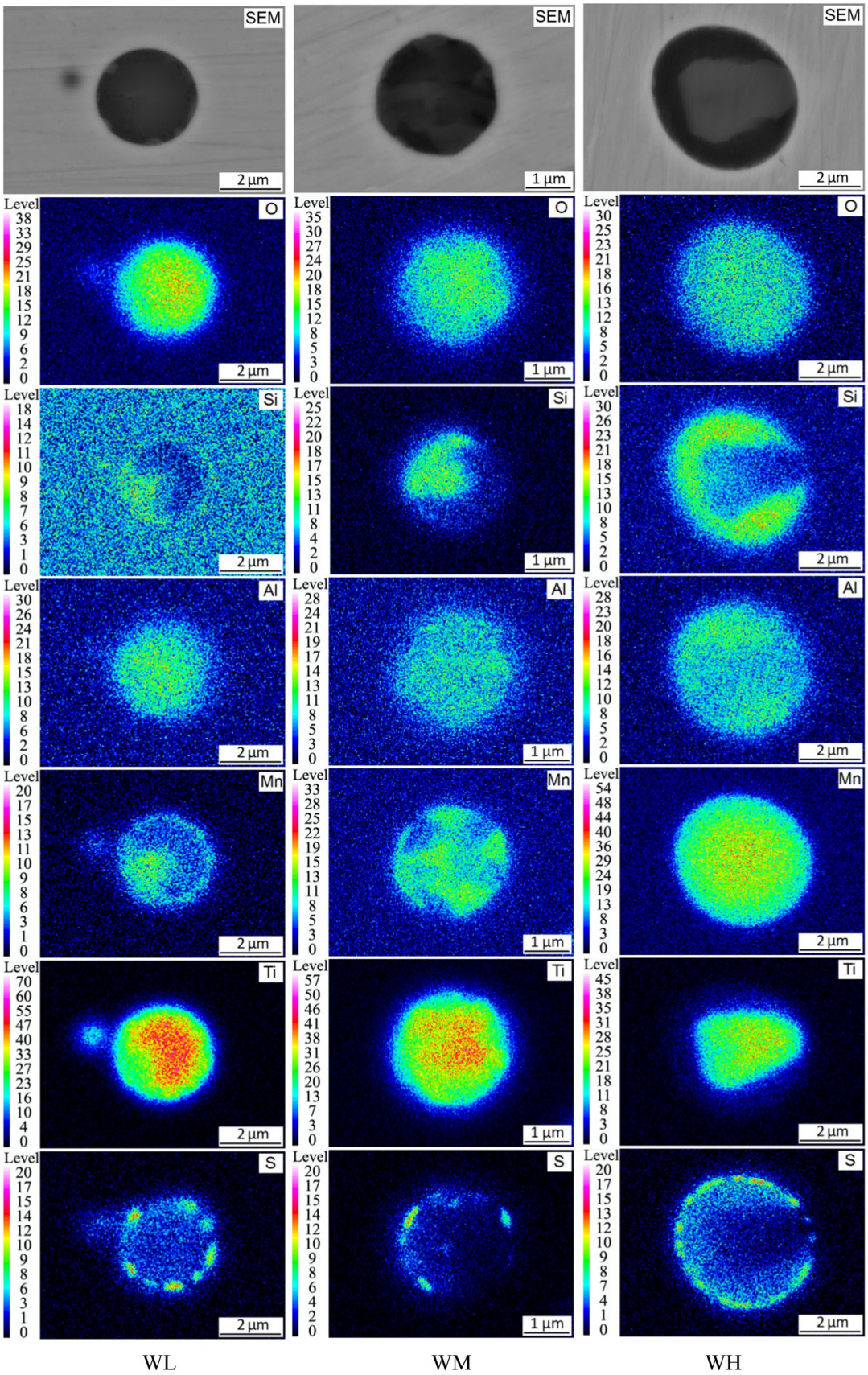


**Fig. 4** EPMA analyses of the inclusions

inclusion are nearly the same as those in WL. Compared with the above weld metals, the (Mn–Si–Al)-oxide content of the inclusion in WH is increased at the expense of (Mn–Ti)-oxide.

Figure 5 demonstrates the thermodynamic analyses of inclusion formation. It is clearly visible that liquid oxide solutions (i.e., molten slags) have been completely disintegrated at 1000 °C. As shown from the constituent phases of the inclusions in WL at this temperature, a large amount of pseudobrookite solid solution is formed in addition to a certain amount of (Mn–Si–Al)-oxide (i.e., $Mn_2Al_4Si_5O_{18}$) and a small amount of mullite. For WM, mullite disappears while a certain amount of spinel is formed, and (Mn–Si–Al)-oxide is changed from $Mn_2Al_4Si_5O_{18}$ to $Mn_3Al_2Si_3O_{12}$. In WH, the content of (Mn–Si–Al)-oxide (i.e., $Mn_3Al_2Si_3O_{12}$) is increased, while pseudobrookite disappears completely. In addition, more ilmenite and spinel are formed.

The constituent contents and chemical compositions of the main solid solutions in the inclusions at 1000 °C were obtained from the thermodynamic analysis results and are shown in Tables 3 and 4, respectively. $Ti_3O_5$, $MnTi_2O_4$ and $MnTiO_3$ are the primary constituents in the respective solid solutions (i.e., pseudobrookite, spinel and ilmenite). It is worth noting that although spinel, ilmenite and pseudobrookite are all Ti-containing solid solutions, spinel and

**Table 3** Constituent contents of the solid solutions (mass%)

| Solid solutions | Constituents | Constituent contents of solid solutions in weld metals with different Mn contents | | |
|---|---|---|---|---|
| | | 0.35% | 1.05% | 2.98% |
| PSEU | $Ti_3O_5$ | 89.9 | 85.8 | – |
| | $MnTi_2O_5$ | 6.25 | 11.4 | – |
| | $FeTi_2O_5$ | 3.17 | 1.95 | – |
| SPIN | $MnTi_2O_4$ | – | 74.2 | 77.5 |
| | $MnAl_2O_4$ | – | 14.7 | 18.3 |
| | $FeTi_2O_4$ | – | 10.5 | 3.82 |
| IlME | $MnTiO_3$ | – | – | 76.5 |
| | $Ti_2O_3$ | – | – | 19.9 |
| | $FeTiO_3$ | – | – | 3.12 |

"–" indicates the absence of a solid solution in weld metals with certain Mn contents

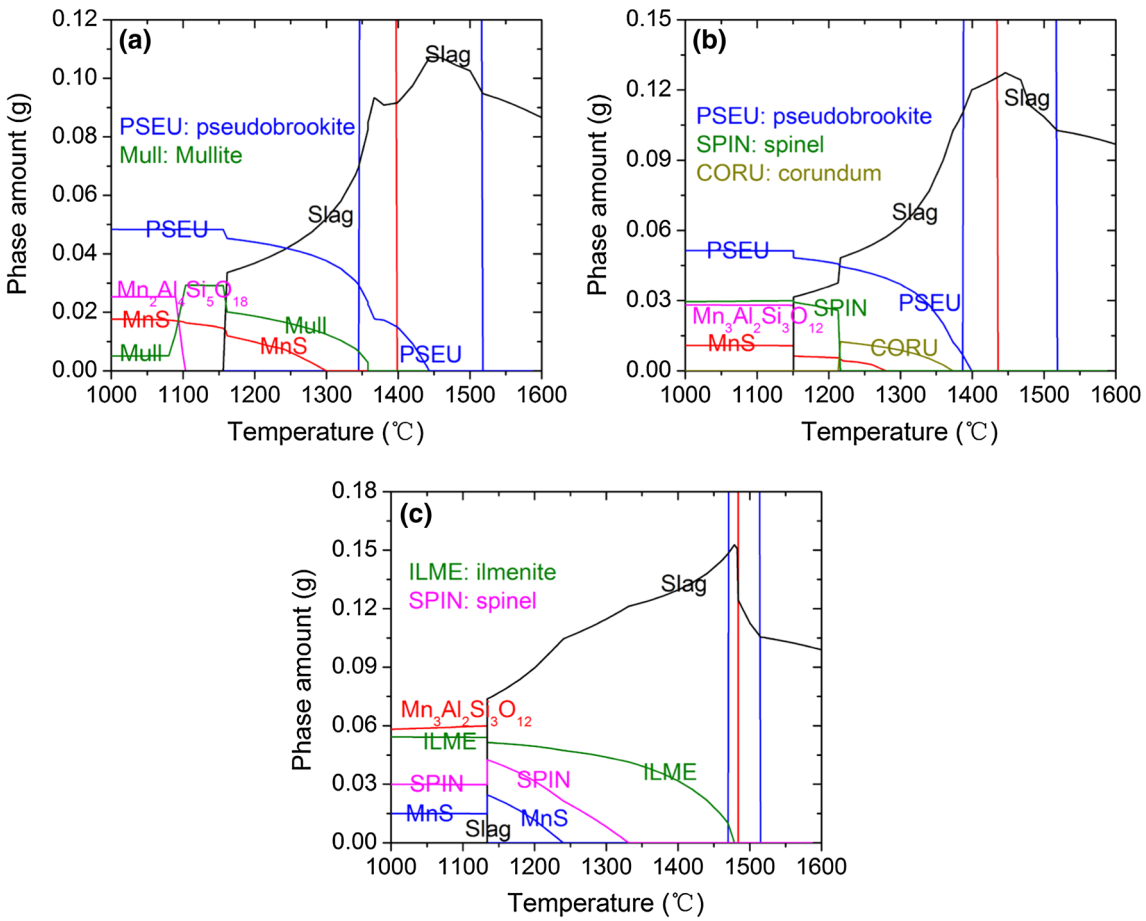


**Fig. 5** Thermodynamic analyses on the inclusion formation for **a** WL, **b** WM and **c** WH

**Table 4** Chemical compositions of the solid solutions (mass%)

| Solid solutions | Elements | Compositions of solid solutions in weld metals with different Mn contents | | |
|---|---|---|---|---|
| | | 0.35% | 1.05% | 2.98% |
| PSEU | O | 36.7 | 36.4 | – |
| | Mn | 2.32 | 3.88 | – |
| | Ti | 60.1 | 59.1 | – |
| SPIN | O | – | 36.7 | 36.4 |
| | Mn | – | 28.1 | 31.6 |
| | Ti | – | 29.9 | 27.3 |
| | Al | – | 2.75 | 3.85 |
| IlME | O | – | – | 31.9 |
| | Mn | – | – | 33.5 |
| | Ti | – | – | 33.8 |

Fe is not listed in Table 4 because its content in its respective solid solutions is very low (less than 1%)

ilmenite have lower Ti contents, but higher Mn contents compared to that of pseudobrookite.

Figures 6 and 7 are TEM analysis results of the typical inclusions, showing the phase identifications in the inclusions using SAED and EDS. It can be seen from the atomic ratios and SAEDs of the constituent phases of Fig. 6 that the (Mn–Ti)-oxide phase in the WL inclusion is pseudobrookite (mainly $Ti_3O_5$), and the (Mn–Si–Al)-oxide in the inclusion should be an amorphous $Mn_2Al_4Si_5O_{18}$ compound.

Similarly, the (Mn–Si–Al)-oxide in the WH inclusion can be identified as an amorphous $Mn_3Al_2Si_3O_{12}$ compound based on the EDS atomic ratio shown in Fig. 7(c1) and the halo pattern shown in Fig. 7(c2). The SAEDs of Figs. 7(b2) and (d2) demonstrate that the (Mn–Ti)-oxide phases in the WH inclusion are ilmenite and spinel solid solutions, respectively. However, these two phases do not seem to be identified from the atomic ratios of the constituent phases in Figs. 7(b1) and (d1); for example, in ilmenite, the atomic ratio (main elements) of Mn:Ti:O is 1:1.6:3.6, not 1:1:3, because these phases are composed of multiple components (for example, $Ti_2O_3$-$FeTiO_3$-$MnTiO_3$ for ilmenite).

Comparisons of Fig. 5 and Tables 3 and 4 with Figs. 4, 6 and 7 show that thermodynamic analyses of the constituents and chemical composition characteristics of inclusions agree well with the experimental results of EPMA maps and TEM analyses. For example, thermodynamic analyses and experimental results all indicate that the inclusion in WL mainly consists of pseudobrookite with a lower Mn level but a higher Ti content compared with ilmenite and spinel, while the inclusion in WH contains large amounts of (Mn–Si–Al)-oxide and ilmenite in addition to a certain amount of spinel.

Moreover, from the SAEDs of Fig. 7e, it can be observed that there is a B-N orientation relationship (namely, $(100)_{Ferrite}//(100)_{MnTi2O4}$ and $[001]_{Ferrite}//[011]_{MnTi2O4}$) between $MnTi_2O_4$ and the adjacent AF, which is consistent with the experimental results of the literature [16, 18]. The B-N orientation relationship of the AF/$MnTi_2O_4$ interface has a low interfacial energy, which contributes to the development of AF by reducing the activation energy of AF nucleation [6, 7].

In addition to the B-N orientation relationship, the presence of the MDZ is another widely recognized mechanism of AF nucleation near inclusions [14–16]. Accordingly, the variation in Mn concentration in the matrix near the inclusions was examined, as shown in Fig. 8. It can be seen that an obvious reduction in the Mn level can be detected around the inclusion containing substantial amounts of ilmenite and spinel solid solutions, whereas no variation in the Mn content is found in the matrix adjacent to the inclusion mainly composed of pseudobrookite and (Mn–Si–Al)-oxide.

As analyzed above, compared with pseudobrookite and (Mn–Si–Al)-oxide, ilmenite and spinel contain higher Mn contents. Therefore, in the case of the formation of large amounts of ilmenite and spinel, Mn around the inclusion can be markedly consumed, resulting in a decrease in Mn concentration in the vicinity of the inclusions. In the case of welding, the cooling rate after welding is very fast, which leads to a very fast solidification of molten metal and solid-state cooling. Thus, the Mn level around inclusions cannot be recovered to an equilibrium state by long-range diffusion of Mn that is far from the inclusions [22]. Consequently, an MDZ develops in the matrix around the inclusions. In brief, the formation of a considerable amount of Mn-rich and Ti-containing phases effectively promotes the development of an MDZ.

As mentioned above, Mn has a remarkable effect on the formation and evolution of inclusions in weld metals. It is common knowledge that various complex metallurgical reactions can occur within the weld pool during welding. The oxygen dissolved in the weld pool can combine with Si, Mn, Ti, Al, etc., which leads to the formation of molten slag (i.e., a variety of liquid oxides, including $Al_2O_3$, $TiO_x$, MnO, etc.) above the liquidus temperature of the molten slag and a drop in the content of the dissolved oxygen in the weld pool. There is a competitive relationship between Si, Mn, Ti, Al, etc., during the oxidation process. In comparison to Mn and Si, Ti and Al possess much stronger affinities with oxygen [23]. Moreover, the amount of the metal elements also has noticeable effects on the oxidation processes of those metals. To clarify the effect of Mn content on the oxidation products, equilibrium calculations on the compositions of liquid oxide solutions at 1450 °C (just before the precipitation of inclusions, as shown in Fig. 5) were carried out with an Fe–0.05C–0.2Si–$x$Mn–0.012Al–0.025Ti–0.04O ($0<x<4$) alloy system (in mass%) similar to the chemical compositions of the weld metals, as shown in Fig. 9. Under low Mn content

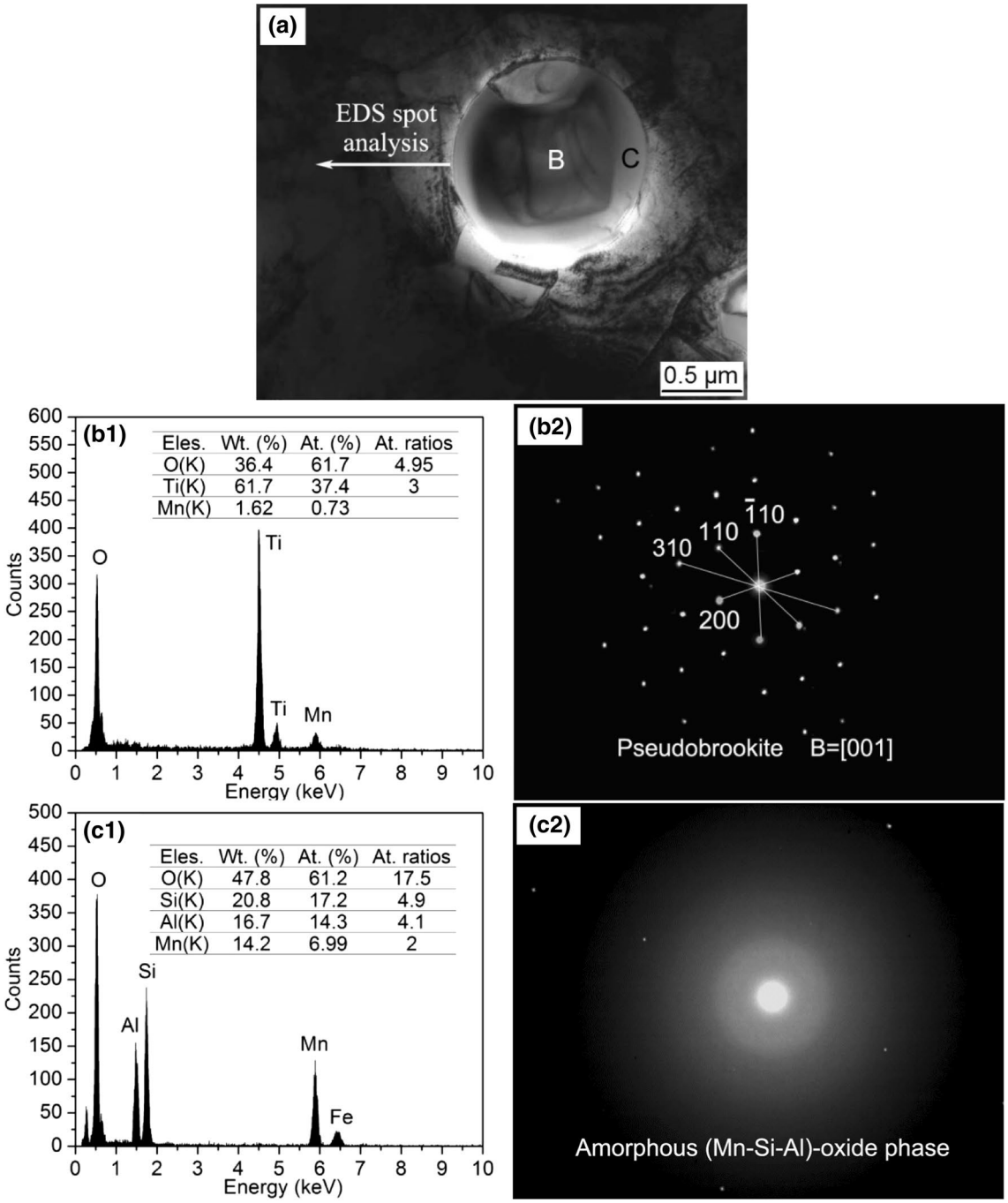


**Fig. 6** TEM analyses for the inclusion in WL: **a** bright field image of inclusion, **b1** and **c1** EDS results taken from regions B and C in (**a**), respectively, and **b2**, **c2** SAEDs obtained from regions B and C in (**a**), respectively

(for example, less than 0.25%), owing to Al and Ti having high affinities with oxygen, the amounts of $Al_2O_3$ and $TiO_x$ (i.e., $Ti_2O_3$ and $TiO_2$) in the oxidation products are higher, while that of MnO is very low. With an increase in Mn content, more Mn can combine with oxygen to consume the oxygen dissolved in the liquid Fe solutions, leading to an increase in the amount of MnO, as shown in Fig. 9. The drop in the amount of oxygen dissolved in the liquid Fe solutions is expected to inhibit the oxidation reactions of the other metal elements, including Al and Ti [24], which results in a drop in the contents of $Al_2O_3$ and $TiO_x$.

During cooling after welding, the inclusions containing different types and contents of constituent phases are precipitated from the molten slags. The amounts of MnO

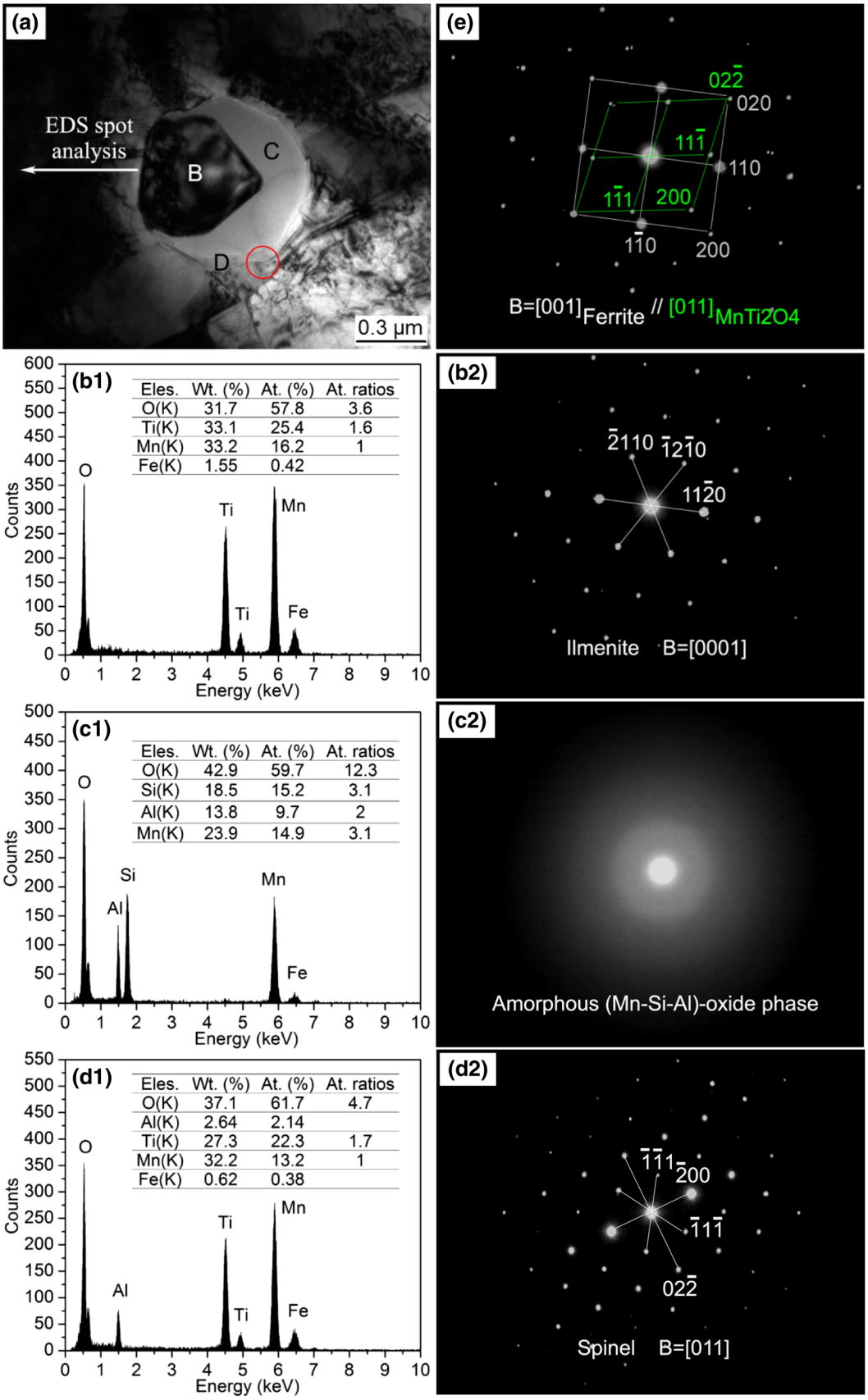
(a)
EDS spot analysis
B
C
D
0.3 μm
(e)
022
020
111
110
111
200
110
200
B=[001]Ferrite // [011]MnTi2O4
(b1)
Eles. Wt. (%) At. (%) At. ratios
O(K) 31.7 57.8 3.6
Ti(K) 33.1 25.4 1.6
Mn(K) 33.2 16.2 1
Fe(K) 1.55 0.42
O
Ti
Mn
Ti
Fe
Counts
Energy (keV)
(b2)
2110 1210
1120
Ilmenite B=[0001]
(c1)
Eles. Wt. (%) At. (%) At. ratios
O(K) 42.9 59.7 12.3
Si(K) 18.5 15.2 3.1
Al(K) 13.8 9.7 2
Mn(K) 23.9 14.9 3.1
O
Si
Al
Mn
Fe
Counts
Energy (keV)
(c2)
Amorphous (Mn-Si-Al)-oxide phase
(d1)
Eles. Wt. (%) At. (%) At. ratios
O(K) 37.1 61.7 4.7
Al(K) 2.64 2.14
Ti(K) 27.3 22.3 1.7
Mn(K) 32.2 13.2 1
Fe(K) 0.62 0.38
O
Al
Ti
Mn
Ti
Fe
Counts
Energy (keV)
(d2)
111
200
111
022
Spinel B=[011]

◂**Fig. 7** TEM analyses for the inclusion in WH: **a** bright field image of inclusion, **b1**–**d1** EDS results taken from regions B–D in **a**, respectively, **b2**–**d2** SAEDs obtained from regions B–D in **a**, respectively, and **e** SAEDs of the circled area in **a**

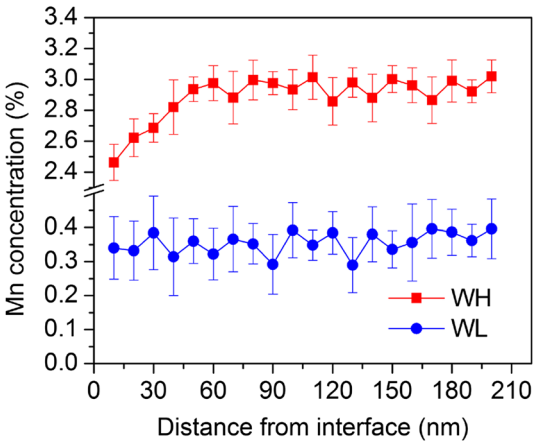


**Fig. 8** Mn concentration profiles for the regions adjacent to the inclusions in Figs. 6a and 7b

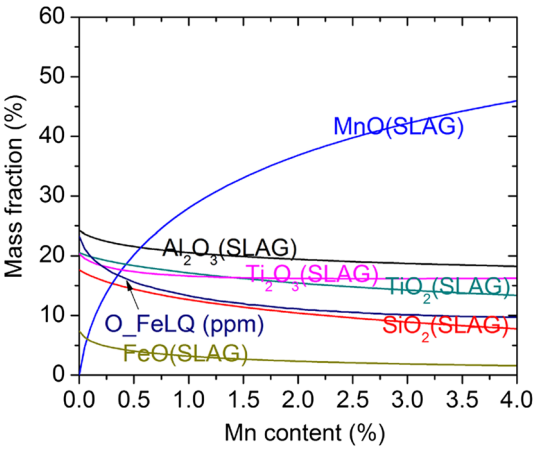


**Fig. 9** Variations in the compositions of liquid oxide solutions with different Mn content at 1450 °C

and $TiO_x$ have remarkable effects on the constituents in the inclusions, especially the kinds of Ti-containing oxide phases. To further demonstrate this effect, slag compositions in an equilibrium at 1450 °C were calculated with the Fe–*x*Mn–0.025Ti–0.04O ($0 < x < 4$) alloy system (in mass%) and superimposed on a ternary isothermal diagram of the MnO-$Ti_2O_3$-$TiO_2$ system at 1000 °C to reveal an inclusion path with varying Mn content, as shown in Fig. 10. With the increase in the amount of MnO (correspondingly, the contents of $TiO_x$ are lowered), the evolution of Ti-containing oxide phases is as follows: pseudobrookite →

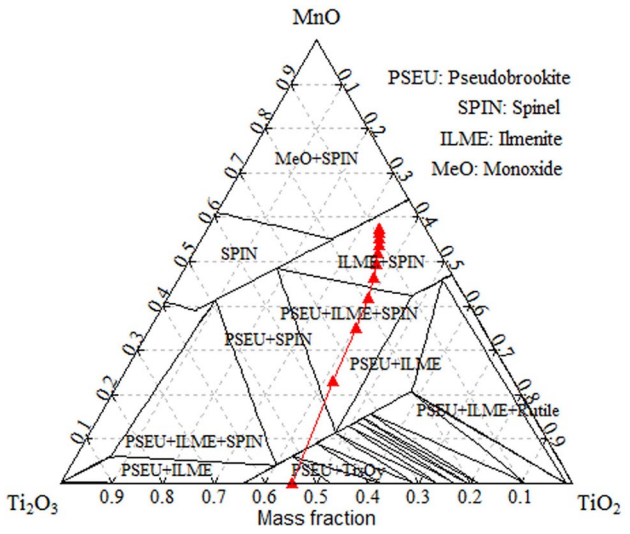


**Fig. 10** Ternary isothermal phase diagram of the MnO–$Ti_2O_3$–$TiO_2$ system at 1000 °C. The red solid line with symbols is the calculated inclusion trajectory with the Fe–*x*Mn–0.025Ti–0.04O ($0 < x < 4$) alloy system (in mass%). (Color figure online)

pseudobrookite + spinel → pseudobrookite + spinel + ilmenite → spinel + ilmenite.

In the case of 0.35% Mn, as analyzed above, the molten slag contains high proportions of $Ti_2O_3$ and $TiO_2$ constituents but a low content of MnO, which promotes the formation of pseudobrookite rather than ilmenite and spinel. Similarly, the formation of (Mn–Si–Al)-oxide is also suppressed due to the low amount of MnO. When the Mn level is increased up to 1.05% and 2.98%, the amounts of $Ti_2O_3$ and $TiO_2$ constituents in molten slag are decreased, but that of MnO is correspondingly increased, which favors the formation of spinel, ilmenite and (Mn–Si–Al)-oxide at the expense of pseudobrookite in the inclusions.

## 4 Conclusions

1. With an increase in Mn content, the primary constituent phases of the inclusions are changed from pseudobrookite to a combination of pseudobrookite and spinel and eventually to a mixture of (Mn–Si–Al)-oxide, spinel and ilmenite.
2. $Ti_3O_5$, $MnTi_2O_4$ and $MnTiO_3$ are the primary constituents of the pseudobrookite, spinel and ilmenite solid solutions, respectively. Spinel and ilmenite have higher amounts of Mn but lower amounts of Ti compared to that of pseudobrookite.
3. In the presence of large amounts of ilmenite and spinel, a Mn-depleted zone is formed in the matrix near the inclusions. Acicular ferrite has a Baker–Nutting orientation relationship with $MnTi_2O_4$.

**Acknowledgements** This study was financially supported by a Project of Education Department of Liaoning Province (Grant No. L2016132). Authors thank Drs. L.Z. Kong (School of Metallurgy of Northeastern University, China) and H.Y. Wu (State Key Laboratory of Rolling & Automation of Northeastern University, China) for providing helps in EPMA, TEM analyses works and thermodynamic calculations.

## References

1. C.K. Lin, Y.C. Pan, Y.H. Frank Su, G.R. Lin, W.S. Hwang, J.C. Kuo, Mater. Charact. **141**, 318 (2018)
2. C.J. Zhang, L.N. Gao, L.G. Zhu, ISIJ Int. **58**, 965 (2018)
3. B.X. Wang, X.H. Liu, G.D. Wang, Metall. Mater. Trans. A **49**, 2124 (2018)
4. J. Pu, S.F. Yu, Y.Y. Li, J. Alloys Compd. **692**, 351 (2017)
5. M.M. Song, B. Song, S.H. Zhang, Z.L. Xue, Z.B. Yang, R.S. Xu, ISIJ Int. **57**, 1261 (2017)
6. T. Yamada, H. Terasaki, Y.I. Komizo, ISIJ Int. **49**, 1059 (2009)
7. A. Takada, Y.I. Komizo, H. Terasaki, T. Yokota, K. Oi, K. Yasuda, Welding Int. **29**, 254 (2015)
8. K. Yamamoto, T. Hasegawa, J.I. Takamura, ISIJ Int. **36**, 80 (1996)
9. K.Y. Seo, Y.M. Kim, H.J. Kim, C.H. Lee, ISIJ Int. **55**, 1730 (2015)
10. Y.B. Kang, H.G. Lee, ISIJ Int. **50**, 501 (2010)
11. J.H. Shim, J.S. Byun, Y.W. Cho, Y.J. Oh, J.D. Shim, D.N. Lee, Scr. Mater. **44**, 49 (2001)
12. J.S. Byun, J.H. Shim, Y.W. Cho, D.N. Lee, Acta Mater. **51**, 1593 (2003)
13. J.H. Shim, Y.W. Cho, S.H. Chung, J.D. Shim, D.N. Lee, Acta Mater. **47**, 2751 (1999)
14. Y.J. Kang, J.H. Jang, J.H. Park, C.H. Lee, Met. Mater. Int. **20**, 119 (2014)
15. Y.J. Kang, K.T. Han, J.H. Park, C.H. Lee, Metall. Mater. Trans. A **45**, 4753 (2014)
16. Y.J. Kang, S.H. Jeong, J.H. Kang, C.H. Lee, Metall. Mater. Trans. A **47**, 2842 (2016)
17. Y.H. Hou, W. Zheng, Z.H. Wu, G.Q. Li, N. Moelans, M.X. Guo, B.S. Khan, Acta Mater. **118**, 8 (2016)
18. H. Nako, H. Hatano, Y. Okazaki, K. Yamashita, M. Otsu, ISIJ Int. **54**, 1690 (2014)
19. L. Cheng, C. Xu, L.L. Lu, L. Yu, K.M. Wu, J. Alloys Compd. **742**, 112 (2018)
20. X.D. Zou, J.C. Sun, D.P. Zhao, H. Matsuura, C. Wang, J. Iron Steel Res. Int. **25**, 164 (2018)
21. X.D. Zou, D.P. Zhao, J.C. Sun, C. Wang, H. Matsuura, Metall. Mater. Trans. B **49**, 481 (2018)
22. Y.J. Kang, K.T. Han, J.H. Park, C.H. Lee, Metall. Mater. Trans. A **46**, 3581 (2015)
23. H. Mitsutaka, I. Kimihisa, *Thermodynamic Data for Steelmaking*, 1st edn. (Tohoku University Press, Sendai, 2010), pp. 232–239
24. K.C. Hsieh, S.S. Babu, J.M. Vitek, S.A. David, Mater. Sci. Eng. A **215**, 84 (1996)